# Hydrogen Bonding in Tight Environments: Simulated Force Spectroscopy of Nanoconfined Hydrogen-Bonded Complexes

Alessandro Pirrotta,[†] Gemma C. Solomon,[†] and Ignacio Franco*,[‡]

[†]Nano-Science Center and Department of Chemistry, University of Copenhagen, 2100, Copenhagen Ø, Denmark
[‡]Department of Chemistry, University of Rochester, Rochester, New York 14627-0216, United States

S *Supporting Information*

ABSTRACT: The single-molecule force spectroscopy of a prototypical class of hydrogen-bonded complexes is computationally investigated. The complexes consist of derivatives of a barbituric acid and a Hamilton receptor that can form up to six simultaneous hydrogen bonds. The force−extension ($F-L$) isotherms of the host−guest complexes are simulated using classical molecular dynamics and the MM3 force field, for which a refined set of hydrogen bond parameters was developed from MP2 *ab initio* computations. The $F-L$ curves

exhibit peaks that signal conformational changes during elongation, the most prominent of which is in the 60−180 pN range and corresponds to the force required to break the hydrogen bonds. These peaks in the $F-L$ curves are shown to be sensitive to relatively small changes in the chemical structure of the host molecule. Thermodynamic insights into the supramolecular assembly were obtained by reconstructing, from the force measurements, the Helmholtz free energy profile along the extension coordinate and decomposing it into energetic and entropic contributions. The complexation is found to be energetically driven and entropically penalized, with the energy contributions overcoming the entropy penalty and driving molecular recognition. Further, the molecular nanoconfinement introduced by the macroscopic surfaces in this class of experiments is shown to significantly accentuate the mechanical and energetic stability of the hydrogen-bonded complexes, thus enhancing the ability of the force spectroscopy to probe this type of molecular recognition events.
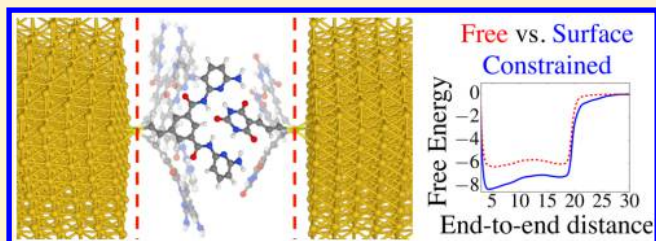
INTRODUCTION

In recent years, a number of techniques have been developed that allow us to access the properties of single molecules.[1−10] These windows into the single-molecule world are teaching us how molecules behave with unprecedented detail, including how they move,[1] their mechanical behavior,[2−5] their conductance,[6,7] reactivity,[8,9] and optical properties.[10] While measurements made on bulk matter are averages over a whole ensemble of molecules, single-molecule measurements highlight the contributions of the constituent parts to the ensemble. Of particular interest here, force-spectroscopy techniques[2−5] can be employed to measure the mechanical properties of single molecules, exert control over the molecular conformation with sub-Ångstrom resolution, and reconstruct the free energy profile during molecular extension. As such, they offer a powerful platform to investigate the forces and thermodynamic changes during basic chemical events such as folding, self-assembly, and molecular recognition.

A scheme of the force-spectroscopy setup using an atomic force microscope (AFM) is shown in Figure 1. In these measurements, one end of a molecule is attached to a macroscopic surface and the other to an AFM tip. The tip is connected to a cantilever of known stiffness k. The distance between the cantilever holder and the surface L is controlled, while the molecular end-to-end distance ξ is allowed to fluctuate. The force F exerted on the molecule is determined by

measuring the deflection of the cantilever with respect to its equilibrium position, i.e., $F = -k(\xi - L)$. During the elongation, L is increased at a constant speed v, $L(t) = L_0 + vt$, and the fluctuating force is recorded.

In this paper, we computationally investigate the utility of single-molecule force spectroscopy as a probe of host−guest molecular recognition events. Specifically, using classical molecular dynamics (MD) and free energy reconstruction techniques we investigate the force spectroscopy characteristics of the hydrogen-bonded (HBed) supramolecular complexes shown in Figure 2, consisting of a Hamilton-like receptor[11,12] host and a barbituric acid derivative guest. For definitiveness, the complexes are thiol-terminated and assumed to be chemisorbed to the macroscopic surfaces. Similar complexes have been synthesized by Gloeckner.[13] These prototypical host−guest complexes have been employed in developing molecular sensors[11,12] and self-assembly strategies.[14−16] Through these complexes we assess the ability of single-molecule force spectroscopy[17−19] to provide information about the basic intermolecular interactions that govern the supramolecular communication events that are important in a variety of drug design, catalysis, and self-assembly applications.[20,21]
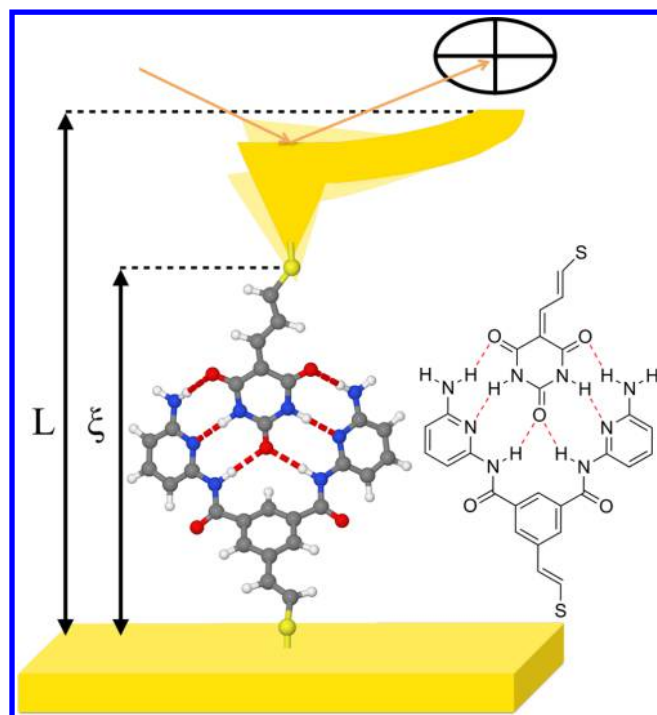
Figure 1. Scheme of an AFM force spectroscopy setup. Here the cantilever holder to surface distance (L) is controlled, while the end-to-end molecular distance (ξ) fluctuates. The force is measured through the deflection of the cantilever from its equilibrium position, $F = -k\,(\xi - L)$ via light scattering from the tip end of the cantilever. For simplicity the finite length of the tip is not taken into account, and the position of the tip is modeled via a dummy atom.

An important difference between measurements of host–guest interactions performed in bulk, with respect to those in single-molecule force spectroscopy, is that in the latter the molecular motion is constrained by the surface and the AFM tip. Such nanoconfinement can have a significant influence on the molecular affinity for complexation[17,22−24] and thus on our

ability to interrogate such events via force measurements. To quantify the effect of nanoconfinement in HBing we consider the force spectroscopy of the complexes in the presence and absence of spatial constraints due to the presence of the surface and tip. As discussed below, nanoconfinement is shown to considerably enhance the free energy of complexation and to increase the force required to break the complexes, thereby increasing the sensitivity of the single-molecule spectroscopy to the molecular interactions responsible for the complexation.

This manuscript is organized as follows. The Methods section describes the employed MD and free energy reconstruction strategy, and introduces a refined set of force field parameters required for the accurate description of hydrogen bond (HB) interactions. The Results and Discussion section discusses the force–extension isotherms of the HB complexes and the influence of chemical changes and spatial constraints on the potential of mean force (PMF). Our main findings are summarized in the Conclusions.

■ METHODS

Molecular Dynamics. The force spectroscopy of the HBed complexes was simulated using classical MD as implemented in TINKER 6.2.[25] The simulations were performed at 300 K in the NVT ensemble using a Nose−Hoover chain[26,27] as a thermostat. The equations of motion were propagated using the modified Beeman algorithm[28−30] with a 1 fs integration time. As a force field we employed MM3[31] (and the MM3-PRO[32] parameters for the amide functional groups in the complexes) supplemented by a refined set of hydrogen bond parameters developed here as described below. The MM3 force field adequately describes π-stacking interactions[33] and includes directional HBing terms[34,35] important in the description of the complexes. The pulling was carried out by attaching the terminal S atom of the host molecule (1) to a stiff isotropic harmonic potential that mimicked the molecular attachment to the surface. Simultaneously, the terminal S of the guest molecule (2) was connected to a dummy atom via a virtual harmonic spring of stiffness $k = 110$ pN Å^{-1}. The distance
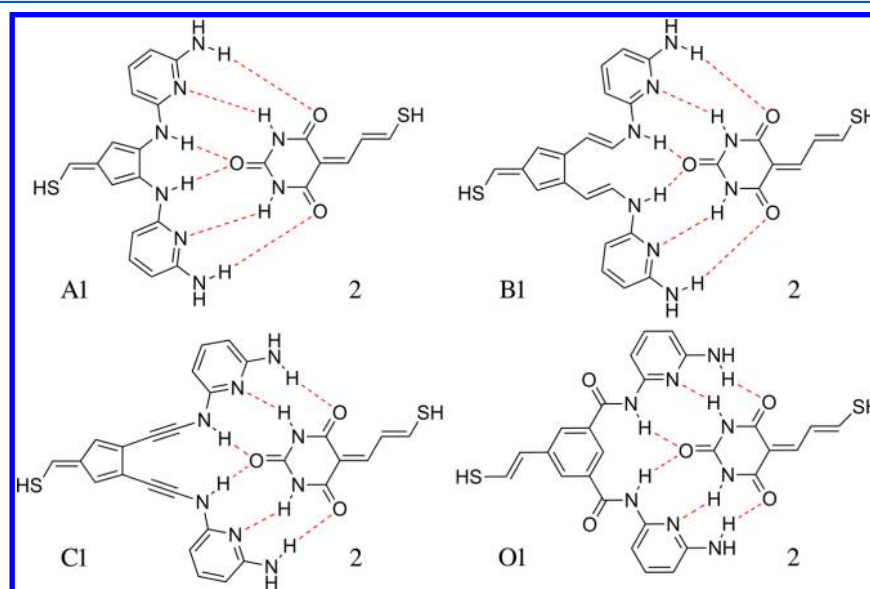

Figure 2. Scheme of the hydrogen-bonded host–guest complexes. The complexes consist of a Hamilton-like receptor host (A1, B1, C1, or O1) and a barbituric acid derivative guest molecule (2). The dashed red lines show the six expected hydrogen bonds in the dimer. Thiol terminations are an example of a functional group that can be used to chemically bond molecules to surfaces.

between this dummy atom and the S in molecule 1 is the simulation equivalent of the distance from the surface to the cantilever-holder L (see Figure 1). In turn, the sulfur-to-sulfur distance defines the end-to-end molecular length ξ. During elongation (or contraction) the dummy atom was moved away from (toward) molecule 1 at a constant speed v, i.e., $L = L_0 + vt$. The rigidity of the cantilever in directions perpendicular to the pulling is captured by restricting the motion of the terminal S atom of molecule 2 to be along the pulling direction. The varying deflection of the virtual harmonic spring measures the force $F = -k(\xi - L)$ exerted during the pulling.

To avoid any dependence of the results on the pulling speed v, the simulations were performed under reversible conditions. To determine the v for which the system effectively behaves reversibly, after 2 ns of thermalization the complexes were stretched from $L = 0$ to 30 Å and subsequently contracted for different pulling speeds in the 10^{-3}–10^{-6} Å ps^{-1} range. A pulling speed of $v = 5 \times 10^{-6}$ Å ps^{-1} was chosen because at this speed (or slower) the force−extension profiles of all complexes during extension and subsequent contraction essentially coincide, indicating that there is no significant dissipation during the pulling. At this v, a full pulling/contraction cycle corresponds to 12 μs of MD simulation time per complex. Molecular structures were dumped every 4 ps, and F, L, ξ, and the molecular potential energy U were recorded and employed to obtain averages. Sampling errors for the force were estimated using the blocking method.[36,37] This method removes the autocorrelation from the data set that causes an underestimation of the standard deviation.

The most prevalent conformations during the pulling were determined via a cluster analysis in VMD.[38] In this analysis, for a given range of ξ (data were binned in 1 Å intervals), the root-mean-square deviation (RMSD) of each structure in the range is calculated with respect to an arbitrary reference. The analysis clusters conformations based on their RMSD and estimates the likelihood of each cluster of structures.

Nanoconfinement. The constraints on molecular motion imposed by the surface and the tip in AFM pulling experiments are modeled via potential restraints. Here, the surface and the tip are considered as impenetrable parallel flat surfaces that are arranged perpendicularly to the pulling direction and separated by a distance ξ. These spatial constraints are effectively implemented via angle restraints that prevent penetration of molecular atoms into the surface regions. Specifically, for atom-i the angle described by the sulfur−atom-i distance vector and the vector normal to the surface to which that particular sulfur is attached to is restricted to be in the $-90° \leq \theta < 90°$ via a stiff harmonic restraint of the form $V(\theta) = \sum_{n=1}^{3} k_n(\theta - \theta_n)^2$ ($Mk_1 = 0.5 \times 10^{-3}$ kcal mol^{-1} rad^{-2}, $\theta_1 = \pm 90°$; $Mk_2 = 1.0 \times 10^{-3}$ kcal mol^{-1} rad^{-2}, $\theta_2 = \pm 80°$; $Mk_3 = 2.0 \times 10^{-3}$ kcal mol^{-1} rad^{-2}, $\theta_3 = \pm 70°$, where M is the number of atoms in the molecular fragment to which the particular atom-i belongs). Results were found to be relatively insensitive to the particular choice of the force constants. However, in the employed computational pulling setup these potential restraints do generate an artificial residual positive force since $(\xi - L) < 0$ even for large L. This residual force is subtracted from the overall force measurements in the nanoconfined simulations.

Refined Hydrogen Bond MM3 Parameters. To accurately describe the HB-mediated intermolecular interactions in the complexes, a set of refined HB MM3 parameters was developed from high-level *ab initio* computations. Specifically, as model molecules for developing the parameter

set we employed the HB complexes T1 and T2 shown in the inset of Figure 3. These molecules were selected because they
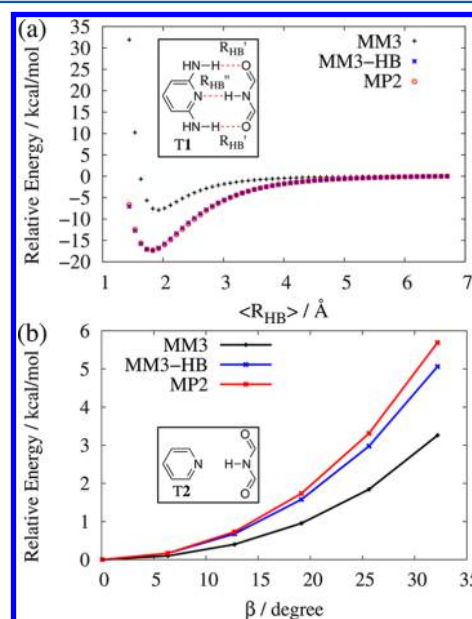

Figure 3. HB interactions described by the MM3-HB and MM3 force field. The plots contrast the MP2 complexation energy with that obtained via MM3 and MM3-HB. (a) Complexation energy of T1 versus average HB distance defined as $\langle R_{HB} \rangle = (R_{N-H} + R_{O-H} + R'_{O-H})/3$. (b) Angular dependence of the complexation energy of T2 around the minimum energy geometry (R_{HB}). Note how MM3-HB accurately describes HB interactions that dominate the dynamics of the complexes in Figure 2.

capture the HB interactions in Figure 2 but are more convenient for high level *ab initio* computations. The geometry of T1 and T2 was first optimized using DFT, the B3LYP exchange and correlation functional,[39] and a 6-311G** basis set.[40] The complementary fragments of the optimized complexes were rigidly separated along the HB axis. The complexation energy along this distance was computed every 0.1 Å using MP2[41] with the aug-cc-pVTZ[42] basis set and the basis set superposition error (BSSE) correction procedure.[43,44] MP2 has been found to accurately describe HB interactions at reasonable computational cost.[45] Here and throughout we employed Gaussian09[46] for the electronic structure computations.

The intermolecular interactions were fitted using the directional HB potential term in MM3[34,35]

$$E_{HB} = \frac{\epsilon_{HB}}{D}\left(a \cdot \exp\left(-b \cdot \frac{R_{Y-H}}{R^\circ_{Y-H}}\right) - c \cdot \left(\frac{R_{X-H}}{R^\circ_{X-H}}\right)\left(\frac{R^\circ_{Y-H}}{R_{Y-H}}\right)^p \cos\beta \right)$$

(1)

where ϵ_{HB} is the HB energy parameter; D is the dielectric constant; R_{Y-H} is the HB distance with equilibrium value R°_{Y-H}; R_{X-H} is the bond length between H and its covalently attached atom with equilibrium bond length R°_{X-H}; and β is the HB angle. The coordinate notation employed in eq 1 is schematically shown in Figure 4. In the fitting, the ϵ_{HB} is kept fixed at the MM3 value, while the dimensionless parameters a, b, and c were all considered as adjustable parameters. While the MM3 force field (FF) employs an asymptotic length dependence $E_{HB} \sim 1/R^6_{Y-H}$ ($p = 6$) akin to van der Waals interactions, here p is considered as a fitting
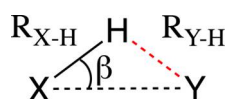
Figure 4. Coordinates in a XH⋯Y HB interaction. Here, R_{Y-H} is the HB distance, R_{X-H} is the X−H covalent bond length, and β is the HB angle.

parameter as the length dependence of HB interactions has been found to exhibit a $p = 3.8$ instead.[47] TINKER was modified to be able to deal with this more general case. The HB parameters for N−H⋯N were fitted from the complexation energy of T2. Then, using these parameters, the HB parameters for N−H⋯O were fitted from the equivalent data for T1. All fitting was performed by a nonlinear least-squares algorithm as implemented in GNUplot.[48] The resulting fitting parameters are shown in Table 1, and the modified FF is denoted as MM3-

Table 1. MM3 and MM3-HB Parameters for NH⋯N and the NH⋯O HB Interactions as Defined by Equation 1

	NH⋯N		NH⋯O	
	MM3	MM3-HB	MM3	MM3-HB
a	184000	9200	184000	2107
b	12.0	6.47	12.0	7.66
c	2.25	24.12	2.25	2.06
p	6	3.8	6	3.8
ϵ_{HB} (kcal/mol)	1.5	1.5	5.24	5.24
R°_{Y-H} (Å)	2.22	1.817	2.22	2.0

HB. Note that for both types of HBs we obtain $p = 3.8$ as a result of the fitting, in agreement with ref 47. A comparison of the complexation energy of T2 computed using MP2, MM3, and MM3-HB is shown in Figure 3a. Note that while the MM3 FF underestimates the HB complexation energy by 48% the MM3-HB FF accurately captures the length dependence in the complexation energy. Further note that the new set of

parameters also leads to an improved description of the directionality of the HBs with respect to that obtained via MM3 (see Figure 3b).

Free Energy Reconstruction. The molecular potential of mean force (PMF) $\phi(\xi)$ along the end-to-end distance coordinate was reconstructed from the biased simulations at extensions L using the weighted histogram analysis method (WHAM),[49,50] as described in detail elsewhere.[4,51] The PMF is the molecular Helmholtz free energy profile along a given coordinate. As such, it is an intrinsic molecular property that is independent of the cantilever stiffness and succinctly captures thermodynamic changes during the complexation. This contrasts with the force measurements, which are generally dependent on k.[4,51] In the WHAM procedure, we employed bins of 0.15 Å along ξ and used as a convergence criteria an average difference of 10^{-5} kcal/mol among consecutive estimates of the free energy in the self-consistent procedure. Errors in the estimate of the PMF were calculated using the bootstrap method.[51] Additional insight into the thermodynamic driving force responsible for the complexation was obtained by decomposing the changes in the PMF into entropic $S(\xi)$ and potential energy $U(\xi)$ contributions, i.e., $\Delta\phi(\xi) = \Delta U(\xi) - T\Delta S(\xi)$. This is done by computing the potential energy along the extension $U(\xi)$ and defining $TS(\xi) \equiv U(\xi) - \phi(\xi)$.

■ RESULTS AND DISCUSSION

Force Spectroscopy. The force spectroscopy of the HBed complexes (cf. Figure 2) is shown in Figure 5. For definitiveness, we focus the discussion on the force−extension ($F-L$) isotherms in the absence of nanoconfinement (dashed lines). The effect of the surface and the tip on the force spectroscopy and the complexation is discussed in "Effect of Nanoconfinement". While the four complexes O, A, B, and C can form the same number and type of HBs, they differ by the central ring of the host molecule 1 and its connection to its two pyridine-based arms. These chemical modifications change the
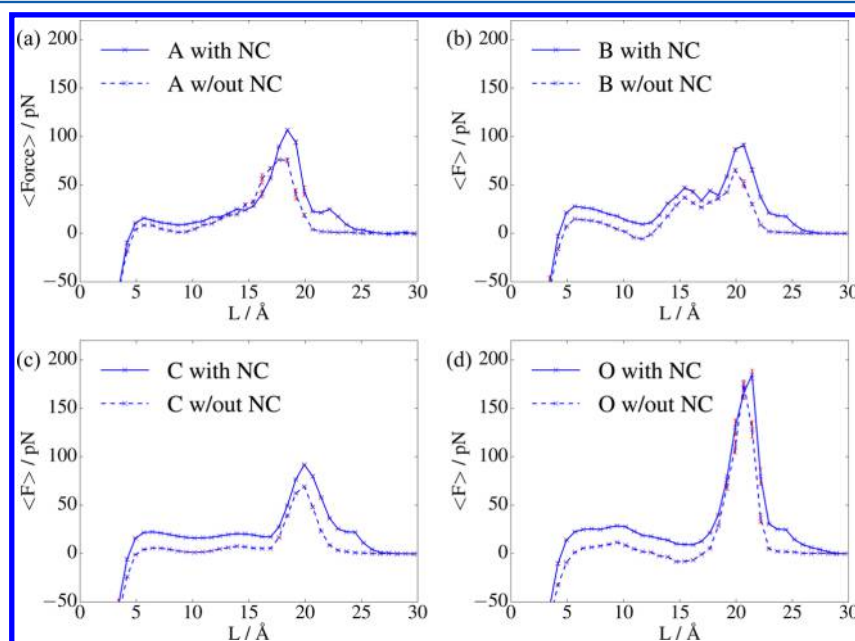

Figure 5. Force versus pulling coordinate during the extension of the complexes in Figure 2 in the presence (solid lines) and absence (dashed lines) of nanoconfinement (NC). Averages are made in 0.75 Å bins. Error bars are shown in red. Note how NC and the chemical structure of the host strongly affect the mechanical stability of HBing.
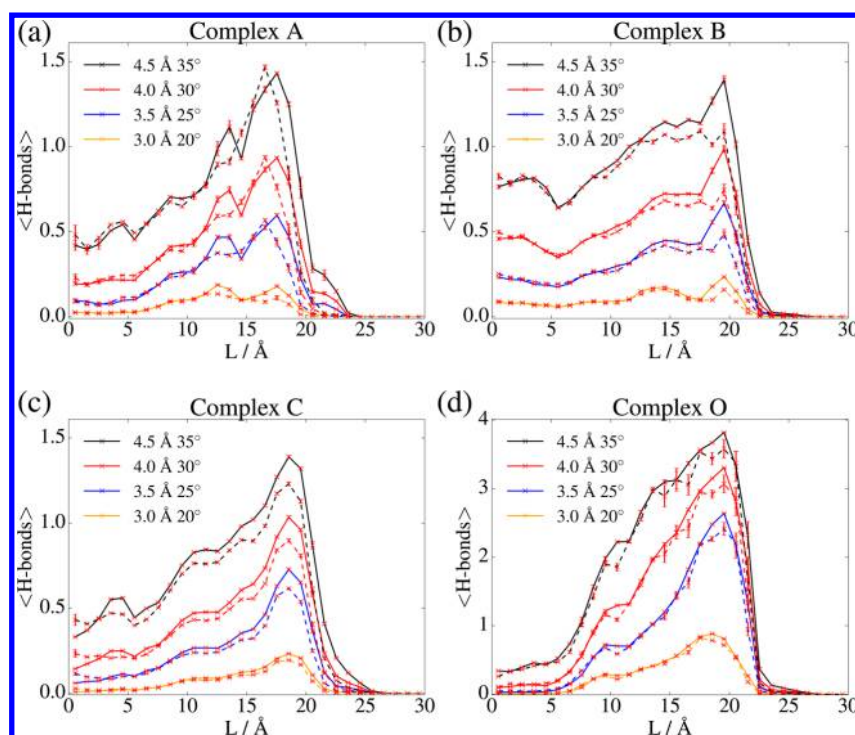
Figure 6. Evolution of HBing during the elongation of the complexes in Figure 2 in the presence (solid lines) and absence (dashed lines) of nanoconfinement. Results are averages over 1 Å bins. Using the notation in Figure 4, a structure is said to be HBed if $R_{Y-H} < R_0$ and $|\beta| < \beta_0$, where R_0 and β_0 are thresholds for the HB distance and angle. Different curves refer to different thresholds as defined in the legends.[38,52] The breaking of HBs is associated with the maximum force in $F-L$ isotherms. Note how thermal fluctuations reduce the average number of HBs from the 6 that are formed by minimum energy conformation, most dramatically in A, B, and C. Note that the y-axis in panel (d) is scaled differently.

flexibility and dimensions of the host that, as discussed below, can dramatically affect the stability of the HBs.

Consider first the $F-L$ isotherm for complex O shown in Figure 5d. The main feature of the isotherm is a peak in the force of 175 pN for $L = 20.7$ Å. The increase in the force and its subsequent drop signal the mechanical deformation and breaking of the complex. Before the main breaking event, for $5 < L < 17$ Å, there is a region in which the force is weakly dependent on the elongation, preceded by a region $L < 5$ Å in which the molecule is compressed leading to a negative force. The average number of intermolecular HBs during the elongation is shown in Figure 6 ((d): complex O; the curves differ by the stringency of the criteria for HBing). An analysis of the molecular conformation during elongation reveals (see "Complexation Thermodynamics" and the representative structures in Figure 7) that in the region where the $F-L$ isotherm is weakly dependent on L the O complex is V shaped (structure 1, Figure 7d). This V-shaped complex is stabilized by dispersion and electrostatic interactions between the fragments. During elongation, complex O flattens, forming the HB-mediated complex detailed by structure 2 in Figure 7d. Subsequent pulling leads to a breaking of the complex.

These geometrical changes during elongation are reflected by the number of HBs the O complex forms as a function of L (Figure 6d). For short extensions, the molecule is stacked and exhibits a low number of HBs. As the molecule is elongated, a structure favorable for HBing is mechanically stabilized, and the number of HBs increases. The maximum in the force coincides with the point in which the largest number of HBs is formed, and the drop in the force is accompanied by the breaking of all HBs in the complex. Thus, the maximum in the force

spectroscopy can be associated with the force required to break the HBs in the complex.

Complexation Thermodynamics. The potential of mean of force (PMF) $\phi(\xi)$ along the molecular end-to-end distance ξ extracted from the mechanically biased simulations is shown in Figure 7 (blue lines). Regions of convexity in $\phi(\xi)$ signal mechanically stable conformations, while regions of concavity signal conformational transitions that lead to mechanical instabilies where the force drops with increased elongation (i.e., $dF/dL < 0$).[4,51] The most prevalent conformations for selected ξ as determined via a cluster analysis (see Methods) are shown in the upper panel of the subfigures.

As can be gleaned from Figure 7d, there are three mechanically stable conformations for complex O interspersed by regions of concavity in $\phi(\xi)$. The conformation around $\xi = 4-5$ Å corresponds to the stacked structure (1). This conformation is followed by the HBed complex (2) and the uncomplexed molecule (3). The global minimum in the free energy corresponds to the stacked complex 1, with the HBed complex being 0.22 kcal/mol higher in free energy. The mechanical instability observed in Figure 5d for $10 < L < 15$ Å is associated with a conformational transition from the stacked structure to the HBed structure. The main region of concavity around $\xi \approx 20$ Å corresponds to the breaking of the HBs in the complex and leads to the main peak in the $F-L$ isotherm.

Additional insight into the thermodynamics of complexation is obtained by decomposing changes in the PMF into energetic and entropic contributions $\Delta\phi(\xi) = \Delta U(\xi) - T\Delta S(\xi)$, as shown in Figure 8. The complexation is energetically driven and entropically penalized, with the energy contributions overcoming the entropy penalty and effectively leading to the molecular recognition event. While the complexation energy
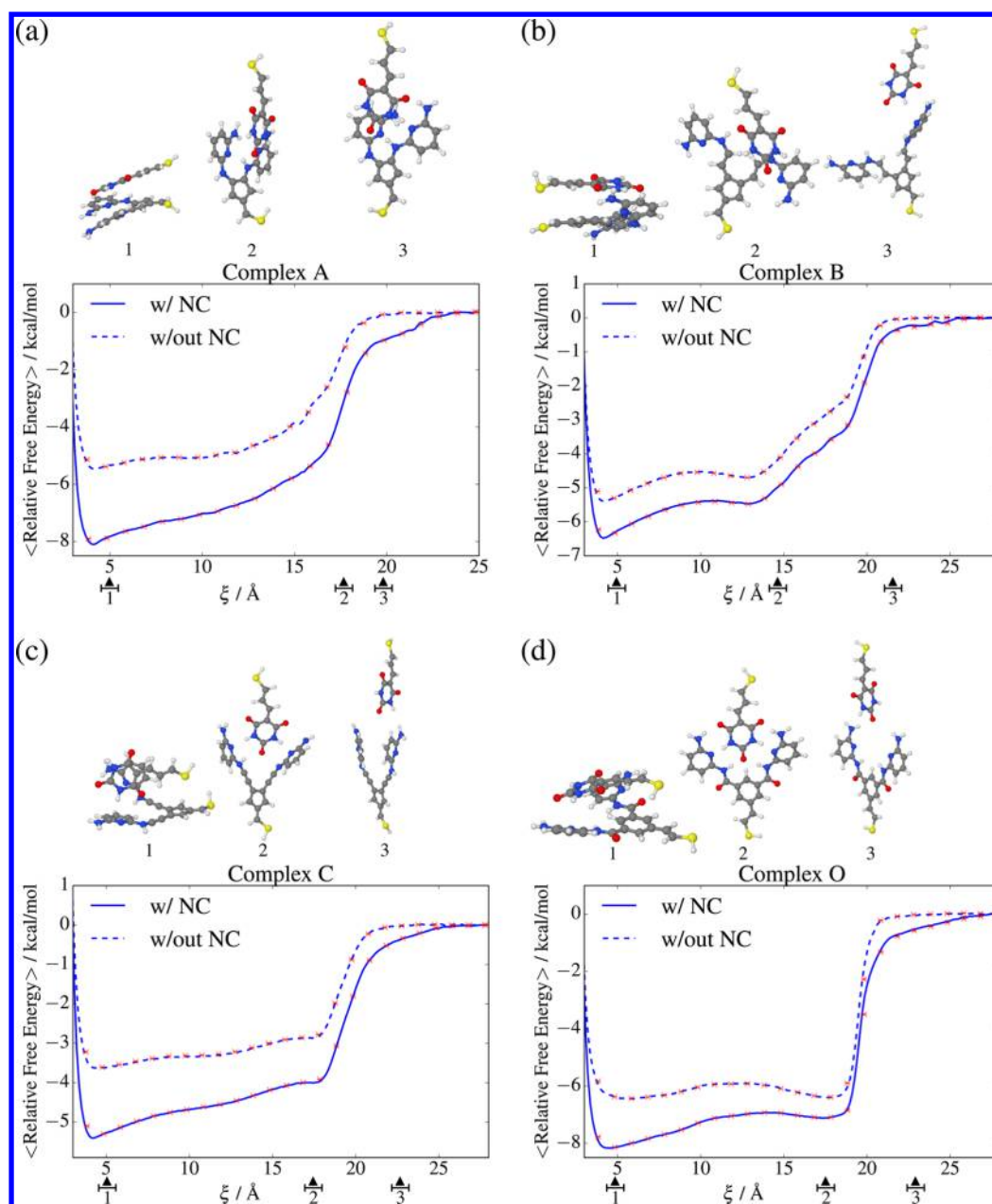
Figure 7. Changes in the potential of mean force ($\phi(\xi)$) along the extension coordinate. Results are shown in the presence (solid lines) and absence (dashed lines) of nanoconfinement (NC) obtained with WHAM using 0.15 Å bins. The red crosses and bootstrap error bars are obtained using a 1 Å bin. Representative structures along the pulling of the system in the absence of nanoconfinement obtained via cluster analysis are shown in the upper panels of each subfigure. The reference free energy was taken to be the complex at a separation of 30 Å. Note how nanoconfinement considerably enhances the complexation.

and entropy vary widely during the extension, these two contributions largely cancel one another leading to only modest changes in the PMF. Note that the HBed structure is significantly more favorable energetically than the stacked conformation. However, it is also associated with a higher entropy penalty due to its highly ordered conformation, which prevents it from being the global minimum in the free energy at 300 K.

Effect of Molecular Structure. Figures 5−7 show that small modifications in the chemical structure of the host can have significant effects on the force spectroscopy and the underlying potential of mean force, highlighting the potential of the technique to probe molecular recognition events. While all complexes exhibit a prominent peak in the $F-L$ isotherms that

is associated with the breaking of the HBs, the magnitude and position of this peak and the details of the $F-L$ behavior reflect the chemical differences between each host−guest environment.

Among the complexes, O forms the largest possible number of HBs (Figure 6), and this leads to the largest force required to break the complex. Specifically, while complexes A, B, and C on average form a maximum of ~1.0−1.5 HBs (using the most lenient of criteria for HBing), complex O forms ~3.5. Further note that thermal fluctuations considerably reduce the average number of HBs that are exhibited by the complexes from the 6 that are expected from minimum energy geometries. In the case of A, this difference is because the host in A is able to form intramolecular HBs (between pyridine N and amino H−N)
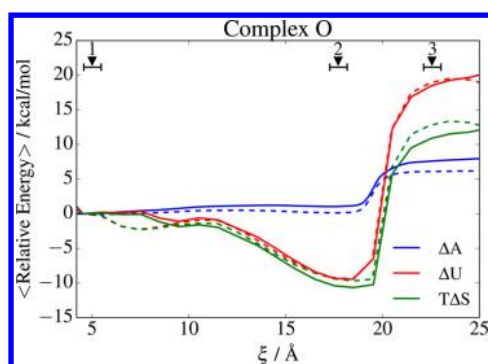
Figure 8. Energy $[U(\xi)]$/entropy $[TS(\xi)]$ decomposition of the potential of mean force $(\Delta\phi(\xi) = \Delta U(\xi) - T\Delta S(\xi))$ of complex O. Results are shown in the presence (solid lines) and absence (dashed lines) of NC. The zero energy reference is taken to be the conformation at $\xi = 4.5$ Å for which the average energy of the complex with and without NC coincides. The numerical labels refer to the representative structures in Figure 7d. The complexation is energetically driven and entropically penalized.

that compete with the intermolecular HBs. Intramolecular HBs are not observed in O because the length between the two arms in the host is longer. In complexes B and C, HBs are typically formed with one arm instead of both under thermal conditions. This is because the flexibility of the arms leads to a strong role of thermal disorder in reducing the number of HBs during the dynamics. Note that minimum energy structures would suggest that all complexes form 6 HBs, while the thermal dynamics show a significantly reduced number of HBs. This fact stresses the importance of taking into account thermal fluctuations, and not just minimum energy geometries, when establishing structure−function relations.

Complexes O, A, and C share a similar shape for the PMF, exhibiting three regions of mechanical stability. Complex B has one additional stable molecular conformation that introduces an extra peak in the $F−L$ isotherm. This extra conformation (not shown) corresponds to a host−guest complex stabilized through dispersion and electrostatic interactions instead of through HBs. In all cases, the stacked conformation corresponds to the global minimum in the free energy. While the complexation energies are comparable (see Table 2) and in

Table 2. Free Energy of Complexation in the Presence and Absence of Nanoconfinement (NC)

complex	$\Delta A_{\text{w/out NC}}$ (kcal/mol)	$\Delta A_{\text{with NC}}$ (kcal/mol)	enhancement (%)
A	-5.73 ± 0.03	-8.0 ± 0.1	39 ± 4
B	-5.22 ± 0.04	-6.40 ± 0.05	23 ± 5
C	-3.71 ± 0.01	-5.40 ± 0.04	46 ± 2
O	-6.29 ± 0.01	-8.22 ± 0.05	31 ± 3

the range of -3.7 to -6.3 kcal/mol, the force required to break complex O is ∼2 larger than in the other cases. Complex O is mechanically more robust because the slope of the PMF just before dissociation is steeper. That is, the transition from HBed to an open structure is sharper than in the other complexes.

Note that an increase in mechanical stability as measured by the maximum force required to break the complexes does not necessarily coincide with a commensurate increase in the free energy of complexation. For example, complexes A and O have similar free energies of complexation of -5.73 and -6.29 kcal/

mol, respectively (see Table 2), but the force required to break complex O is ∼2.4 larger. The reason for this is because while the mechanical stability is determined by the force required to break the hydrogen bonds the complexation is governed by the free energy difference between the compact stacked conformation and the uncomplexed molecule.

Effect of Nanoconfinement. Nanoconfinement enhances the mechanical stability and the complexation energy of all complexes. In fact, for $L = 0−15$ Å the force required to extend the complex increases by ∼10−20 pN. Further, the force required to break the complexes increases by ∼15−30 pN. This overall increase in the force implies that the nanoconfined complexes are thermodynamically and mechanically more stable. Note that the free energy of complexation (see Table 2) increases by 23−46% upon nanoconfinement. The surface and tip lead to an enhancement in the number of HBs observed overall (as measured by the areas under the curves in Figure 6). In addition, the NC introduces a secondary peak in the force spectroscopy after the main dissociation event. This peak arises because of HB interactions between the central carbonyl group in the guest and the terminal NH_2 groups in the arms of the host that are now favored by this environment. That is, the tight environment imposed by the surface and the tip in this class of experiments makes the complexes more stable and less prone to mechanical rupture and the force spectroscopy more sensitive to molecular recognition events.

The energy/entropy decomposition of the PMF shown in Figure 8 shows that the NC can affect both the potential energy and entropy of the complex along ξ. In the particular case of the O complex, the NC leaves the potential energy essentially unaltered in the 10 Å $< \xi <$ 24 Å range. By contrast, the NC reduces the entropy of the dimer in both open and complexed form because of constraints in motion imposed by the surfaces. This reduction of entropy is seen to be more significant for the open complex than for the interacting complex, and this factor is seen to play a main role in the stabilization of the O complex by the tight environment. More generally, the stabilization results from the nontrivial competition between enhanced interactions and possible entropy reductions due to constraints in molecular motion. This interplay results in different enhancements in the complexation energy of the different model dimers by 23% to 46% (cf. Table 2).

These results are consistent with previous computational observations[22] where surface constraints were seen to enhance the complexation free energy of a β-cyclodextrin/ferrocene complex. Results in ref 22 suggest that this type of enhancement in the complexation are also robust to possible solvent effects.

■ CONCLUSIONS

We have investigated the ability of single-molecule force spectroscopy to provide information about molecular communication events through supramolecular interactions. For this, we simulated the force spectroscopy of the class of hydrogen-bonded complexes shown in Figure 2. During elongation, these complexes transition from a compact stacked conformation into a hydrogen-bonded structure and eventually break. The maxima in the force signal conformational transitions, and the main peak signals the breaking of the intermolecular hydrogen bonds that mechanically stabilize the complex.

The force spectroscopy is shown to be sensitive to details in the chemical structure in the host molecule. These chemical changes influence the position and magnitude of the peaks in

the force and the shape of the underlying potential of mean force along the extension coordinate. Further, the molecular nanoconfinement inherent to this class of measurements is shown to significantly enhance the free energy of formation and the mechanical stability of the complexes, thereby increasing the sensitivity of the spectroscopy to the single-molecule molecular events responsible for complexation.

A decomposition of the potential of mean force into energetic and entropic contributions indicates that the complexation is energetically driven and entropically penalized. While the hydrogen-bonded structure is by far the most energetically favored conformation, its ordered structure is associated with an entropy penalty that prevents it from being the room-temperature native conformation.

These results apply to the idealized situation where the solvent plays a minor role on the MD, where the impenetrable surfaces have no other nonbonded interactions with the molecule and where the radius of the AFM tip is large with respect to the molecular scale. Polar solvents will qualitatively influence the results by introducing competition for HBing. Further, any attractive interactions between the molecule and the surfaces will reduce the effect of nanoconfinement. Similarly, employing atomically sharp tips or linker groups between the tip/surface and the complex are also expected to reduce the effect of nanoconfinement because they increase the conformational freedom of the molecule with respect to the situation considered.

The simulations highlight the ability of force measurements to discern between molecular recognition events, stress the importance of taking into account thermal fluctuations (and not just minimum energy geometries) when establishing structure–function relations, and exemplify how novel environments can distort basic molecular interactions responsible for molecular assembly and recognition.

■ ASSOCIATED CONTENT

ⓢ Supporting Information

The Supporting Information is available free of charge on the ACS Publications website at DOI: 10.1021/acs.jpcc.6b06823.

Movie of the simulated elongation of complex O with nanoconfinement under reversible conditions (MPG)

■ AUTHOR INFORMATION

Corresponding Author
*E-mail: ignacio.franco@rochester.edu. Phone: +1 585 275 8209.

Notes
The authors declare no competing financial interest.

■ ACKNOWLEDGMENTS

■ REFERENCES

(1) Moerner, W. E. Nobel Lecture: Single-Molecule Spectroscopy, Imaging, and Photocontrol: Foundations for Super-Resolution Microscopy. *Rev. Mod. Phys.* **2015**, *87*, 1183−1212.

(2) Neuman, K. C.; Nagy, A. Single-Molecule Force Spectroscopy: Optical Tweezers, Magnetic Tweezers and Atomic Force Microscopy. *Nat. Methods* **2008**, *5*, 491−505.

(3) Rief, M.; Gautel, M.; Oesterhelt, F.; Fernandez, J. M.; Gaub, H. E. Reversible Unfolding of Individual Titin Immunoglobulin Domains by AFM. *Science* **1997**, *276*, 1109−1112.

(4) Franco, I.; Ratner, M. A.; Schatz, G. C. In *Nano and Cell Mechanics*; Espinosa, H. D., Bao, G., Eds.; John Wiley & Sons, Ltd.: New York, 2013; pp 359−388.

(5) Woodside, M. T.; Block, S. M. Reconstructing Folding Energy Landscapes by Single-Molecule Force Spectroscopy. *Annu. Rev. Biophys.* **2014**, *43*, 19−39.

(6) Gimzewski, J. K.; Christian, J. Nanoscale Science of Single Molecules Using Local Probes. *Science* **1999**, *283*, 1683−1688.

(7) Bergfield, J. P.; Ratner, M. A. Forty Years of Molecular Electronics: Non-Equilibrium Heat and Charge Transport at the Nanoscale. *Phys. Status Solidi B* **2013**, *250*, 2249−2266.

(8) Aragonès, A. C.; Haworth, N. L.; Darwish, N.; Ciampi, S.; Bloomfield, N. J.; Wallace, G. G.; Diez-Perez, I.; Coote, M. L. Electrostatic Catalysis of a Diels-Alder Reaction. *Nature* **2016**, *531*, 88−91.

(9) Schuler, B.; Fatayer, S.; Mohn, F.; Moll, N.; Pavliček, N.; Meyer, G.; Peña, D.; Gross, L. Reversible Bergman Cyclization by Atomic Manipulation. *Nat. Chem.* **2016**, *8*, 220−224.

(10) Le Ru, E. C.; Etchegoin, P. G. Single-Molecule Surface-Enhanced Raman Spectroscopy. *Annu. Rev. Phys. Chem.* **2012**, *63*, 65−87.

(11) Chang, S. K.; Hamilton, A. D. Molecular Recognition of Biologically Interesting Substrates: Synthesis of an Artificial Receptor for Barbiturates Employing Six Hydrogen Bonds. *J. Am. Chem. Soc.* **1988**, *110*, 1318−1319.

(12) Chang, S. K.; Van Engen, D.; Fan, E.; Hamilton, A. D. Hydrogen Bonding and Molecular Recognition: Synthetic, Complexation, and Structural Studies on Barbiturate Binding to an Artificial Receptor. *J. Am. Chem. Soc.* **1991**, *113*, 7640−7645.

(13) Glockner, C.; Lüning, U. A Conjugated Hydrogen Bond Receptor for Attachment to Gold. *J. Inclusion Phenom. Macrocyclic Chem.* **2011**, *71*, 239−242.

(14) Yang, S. K.; Zimmerman, S. C. Hydrogen Bonding Modules for Use in Supramolecular Polymers. *Isr. J. Chem.* **2013**, *53*, 511−520.

(15) Dirksen, A.; Hahn, U.; Schwanke, F.; Nieger, M.; Reek, J. N. H.; Vögtle, F.; De Cola, L. Multiple Recognition of Barbiturate Guests by "Hamilton- Receptor"- Functionalized Dendrimers. *Chem. - Eur. J.* **2004**, *10*, 2036−2047.

(16) Wessendorf, F.; Gnichwitz, J.-F.; Sarova, G. H.; Hager, K.; Hartnagel, U.; Guldi, D. M.; Hirsch, A. Implementation of a Hamiliton-Receptor-Based Hydrogen-Bonding Motif toward a New Electron Donor-Acceptor Prototype: Electron versus Energy Transfer. *J. Am. Chem. Soc.* **2007**, *129*, 16057−16071.

(17) Auletta, T.; De Jong, M. R.; Mulder, A.; van Veggel, F. C. J. M.; Huskens, J.; Reinhoudt, D. N.; Zou, S.; Zapotoczny, S.; Schönherr, H.; Vancso, G. J.; Kuipers, L. β-Cyclodextrin Host-Guest Complexes Probed under Thermodynamic Equilibrium: Thermodynamics and AFM Force Spectroscopy. *J. Am. Chem. Soc.* **2004**, *126*, 1577−1584.

(18) Borrell, J. H.; Montero, M. T.; Morros, A.; Domènech, Ò. Unspecific Membrane Protein-Lipid Recognition: Combination of AFM Imaging, Force Spectroscopy, DSC and FRET Measurements. *J. Mol. Recognit.* **2015**, *28*, 679−686.

(19) Dammer, U.; Hegner, M.; Anselmetti, D.; Wagner, P.; Dreier, M.; Huber, W.; Güntherodt, H. J. Specific Antigen/Antibody Interactions Measured by Force Microscopy. *Biophys. J.* **1996**, *70*, 2437−2441.

(20) Steed, J. W.; Atwood, J. L. *Supramolecular Chemistry*; John Wiley & Sons, Ltd., 2009.

(21) Persch, E.; Dumele, O.; Diederich, F. Molecular Recognition in Chemical and Biological Systems. *Angew. Chem., Int. Ed.* **2015**, *54*, 3290−3327.

(22) Filippini, G.; Goujon, F.; Bonal, C.; Malfreyt, P. Energetic Competition Effects on Thermodynamic Properties of Association

between β-CD and Fc Group: A Potential of Mean Force Approach. *J. Phys. Chem. C* **2012**, *116*, 22350−22358.

(23) Filippini, G.; Bonal, C.; Malfreyt, P. Why is the Association of Supramolecular Assemblies Different under Homogeneous and Heterogeneous Conditions? *Phys. Chem. Chem. Phys.* **2012**, *14*, 10122−10124.

(24) Keten, S.; Zhiping, X.; Ihle, B.; Buehler, M. J. Nanoconfinement Controls Stiffness, Strength and Mechanical Toughness of β-Sheet Crystals in Silk. *Nat. Mater.* **2010**, *9*, 359−367.

(25) Ponder, J. W. *TINKER*, version 6.2; Washington University: St. Louis, MO, 2013.

(26) Nosé, S. A Unified Formulation of the Constant Temperature Molecular Dynamics Methods. *J. Chem. Phys.* **1984**, *81*, 511−519.

(27) Hoover, W. G. Canonical Dynamics: Equilibrium Phase-Space Distributions. *Phys. Rev. A* **1985**, *31*, 1695−1697.

(28) Schofield, P. Computer Simulation Studies of the Liquid State. *Comput. Phys. Commun.* **1973**, *5*, 17−23.

(29) Beeman, D. Some Multistep Methods for Use in Molecular Dynamics Calculations. *J. Comput. Phys.* **1976**, *20*, 130−139.

(30) Levitt, M.; Meirovitch, H. Integrating the Equations of Motion. *J. Mol. Biol.* **1983**, *168*, 617−620.

(31) Allinger, N. L.; Yuh, Y. H.; Lii, J. H. Molecular Mechanics. The MM3 Force Field for Hydrocarbons. 1. *J. Am. Chem. Soc.* **1989**, *111*, 8551−8566.

(32) Lii, J. H.; Allinger, N. L. The MM3 Force Field for Amides, Polypeptides and Proteins. *J. Comput. Chem.* **1991**, *12*, 186−199.

(33) Franco, I.; Ratner, M. A.; Schatz, G. C. Coulombic Interactions and Crystal Packing Effects in the Folding of Donor-Acceptor Oligorotaxanes. *J. Phys. Chem. B* **2011**, *115*, 2477−2484.

(34) Lii, J. H.; Allinger, N. L. Directional Hydrogen Bonding in the MM3 Force Field: I. *J. Phys. Org. Chem.* **1994**, *7*, 591−609.

(35) Lii, J. H.; Allinger, N. L. Directional Hydrogen Bonding in the MM3 Force Field: II. *J. Comput. Chem.* **1998**, *19*, 1001−1016.

(36) Flyvbjerg, H.; Petersen, H. G. Error Estimates on Averages of Correlated Data. *J. Chem. Phys.* **1989**, *91*, 461.

(37) Spencer, J. Pyblock: a Python Module for Performing a Reblocking Analysis on Serially-Correlated Data. Accessed 16/11/2015. http://github.com/jsspencer/pyblock.

(38) Humphrey, W.; Dalke, A.; Schulten, K. VMD: Visual Molecular Dynamics. *J. Mol. Graphics* **1996**, *14*, 33−38.

(39) Becke, A. D. Density-Functional Thermochemistry. III. The Role of Exact Exchange. *J. Chem. Phys.* **1993**, *98*, 5648.

(40) Krishnan, R.; Binkley, J. S.; Seeger, R.; Pople, J. A. Self-Consistent Molecular Orbital Methods. XX. A Basis Set for Correlated Wave Functions. *J. Chem. Phys.* **1980**, *72*, 650−654.

(41) Møller, C.; Plesset, M. S. Note on an Approximation Treatment for Many-Electron Systems. *Phys. Rev.* **1934**, *46*, 618−622.

(42) Dunning, T. H. Gaussian Basis Sets for Use in Correlated Molecular Calculations. I. The Atoms Boron through Neon and Hydrogen. *J. Chem. Phys.* **1989**, *90*, 1007−1023.

(43) Boys, S. F.; Bernardi, F. The Calculation of Small Molecular Interactions by the Differences of Separate Total Energies. Some Procedures with Reduced Errors. *Mol. Phys.* **1970**, *19*, 553−566.

(44) Simon, S.; Duran, M.; Dannenberg, J. J. How Does Basis Set Superposition Error Change the Potential Surfaces for Hydrogen-Bonded Dimers? *J. Chem. Phys.* **1996**, *105*, 11024.

(45) Riley, K. E.; Hobza, P. Assessment of the MP2 Method, along with Several Basis Sets, for the Computation of Interaction Energies of Biologically Relevant Hydrogen Bonded and Dispersion Bound Complexes. *J. Phys. Chem. A* **2007**, *111*, 8257−8263.

(46) Frisch, M. J.; Trucks, G. W.; Schlegel, H. B.; Scuseria, G. E.; Robb, M. A.; Cheeseman, J. R.; Scalmani, G.; Barone, V.; Mennucci, B.; Petersson, G. A. *Gaussian 09*, Revision B.1; Gaussian, Inc.: Wallingford, CT, 2010.

(47) Wendler, K.; Thar, J.; Zahn, S.; Kirchner, B. Estimating the Hydrogen Bond Energy. *J. Phys. Chem. A* **2010**, *114*, 9529−9536.

(48) Williams, T.; Kelle, C. *GNUplot*, version 4.4; An Interactive Plotting Program, 2011.

(49) Ferrenberg, A. M.; Swendsen, R. H. Optimized Monte Carlo Data Analysis. *Phys. Rev. Lett.* **1989**, *63*, 1195−1198.

(50) Kumar, S.; Rosenberg, J. M.; Bouzida, D.; Swendsen, R. H.; Kollman, P. A. THE Weighted Histogram Analysis Method for Free-Energy Calculations on Biomolecules. I. The Method. *J. Comput. Chem.* **1992**, *13*, 1011−1021.

(51) Franco, I.; Schatz, G. C.; Ratner, M. A. Single-Molecule Pulling and the Folding of Donor-Acceptor Oligorotaxanes: Phenomenology and Interpretation. *J. Chem. Phys.* **2009**, *131*, 124902.

(52) Gumbart, J. C.; Luo, D. *HBonds Plugin*, version 1.2.